

Supporting Information

## Demonstration of a 50 cm<sup>2</sup> BiVO<sub>4</sub> Tandem Photoelectrochemical-Photovoltaic Water Splitting Device

Ibbi Y. Ahmet,<sup>‡,a</sup> Yimeng Ma,<sup>‡,a</sup> Ji-Wook Jang,<sup>a</sup> Tobias Henschel,<sup>b</sup> Bernd Stannowski,<sup>b</sup> Tânia Lopes,<sup>c</sup> António Vilanova,<sup>c</sup> Adélio Mendes,<sup>c</sup> Fatwa F. Abdi\*<sup>a</sup> and Roel van de Krol\*<sup>a</sup>

<sup>a</sup> Institute for Solar Fuels, Helmholtz-Zentrum Berlin für Materialien und Energie GmbH, Hahn-Meitner-Platz 1, 14109 Berlin, Germany. Email: [fatwa.abdi@helmholtz-berlin.de](mailto:fatwa.abdi@helmholtz-berlin.de), [roel.vandekrol@helmholtz-berlin.de](mailto:roel.vandekrol@helmholtz-berlin.de)

<sup>b</sup> PVcomB, Helmholtz-Zentrum Berlin für Materialien und Energie GmbH, Schwarzschildstr. 3, 12489 Berlin, Germany

<sup>c</sup> LEPABE – Faculty of Engineering, University of Porto, Rua Dr. Roberto Frias, 4200-465 Porto, Portugal

## Supporting Information

### Supplementary Note S1: Internal resistance model

One of the simplest ways to model resistive losses in a large-area photoelectrochemical cell is to capture all losses in a single internal resistance,  $R_{int}$ . The model, which is illustrated in Figure S1, further assumes that both the potential ( $V_s$ ) and the photocurrent density ( $J_s$ ) at the surface of the photoelectrode are the same everywhere. In other words, there are no voltage losses within the photoelectrode itself. The potential at the surface is then given by

$$V_s = V_{appl} - V_{loss} \quad (\text{S1})$$

$V_{appl}$  is the voltage applied by the potentiostat. The voltage loss due to the internal resistance is given by

$$V_{loss} = I_{tot}R_{int} = J_s A R_{int} \quad (\text{S2})$$

Where  $I_{tot}$  is the total current produced by the photoelectrode and  $A$  is the surface area of the photoelectrode. Combining (S1) and (S2) gives

$$V_s = V_{appl} - J_s A R_{int} \quad (\text{S3})$$

Equation (S3) can only be solved iteratively since the photocurrent density,  $J_s$ , depends on  $V_s$  itself. We therefore rewrite (S3) as

$$V_{appl} = V_s + J_s A R_{int} \quad (\text{S4})$$

Experimentally measured values for  $V_s$  and  $J_s$  are available in the form of photocurrent data for small area photoelectrodes. The curves in Fig. 2 are obtained by calculating  $V_{appl}$  from the data for the  $0.24 \text{ cm}^2$   $\text{BiVO}_4$  photoelectrode (solid black curve in Fig. 1) and by plotting  $J_s$  as a function of  $V_{appl}$ .

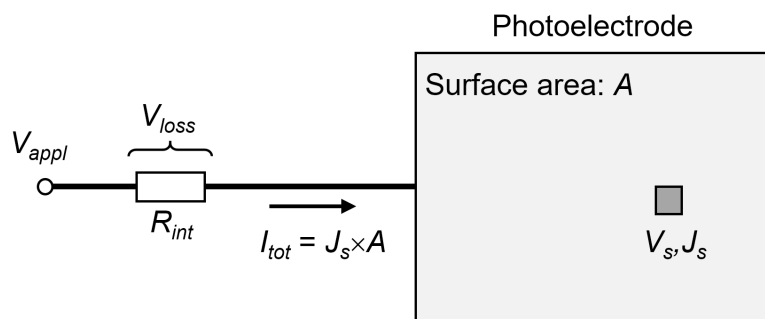


**Figure S1.** Illustration of the simple internal resistance model, in which all resistive losses in the system are captured in a single resistance value. Larger photoelectrodes generate higher currents and, therefore, have larger internal voltage losses.

## Supporting Information

### **Supplementary Note S2: Simulation of the potential drop distributed across TEC 7 FTO for Photo-electrode of various geometries with specific photocurrent densities**

**Software used to Run the Simulation:** QuickField Student Edition 6.3

**Simulation Model:** DC Conductive Model

#### **Model Descriptions and Boundary Conditions:**

The potential drop across a thin film of TEC 7 FTO was simulated based on the following conditions:

1. A rectangular prism is defined for the FTO layer, with a total width (x) of 7 cm and length (y) of 12 cm (see Fig. S2 A), based on the real geometry of the FTO used in our experiments. The actual thickness of our FTO layer is ~300 nm, however constructing this geometry results in the generation of a large number of vector nodes and meshing complexity. A pseudo-thickness (z) of 0.25 cm is therefore used, and the conductivity value is scaled accordingly; effective conductivity of  $57.12 \text{ S m}^{-1}$  is used in our 0.25 cm thick FTO domain, calculated based on the real conductivity of our TEC 7 FTO ( $4.76 \times 10^5 \text{ S m}^{-1}$ ; sheet resistance of  $7 \Omega/\square$ )<sup>1</sup> divided by the ratio between the pseudo-thickness and the real-thickness (0.25 cm / 300 nm). For the small area electrode ( $0.24 \text{ cm}^2$ ), a smaller pseudo-thickness of 1 mm could be used and therefore the effective conductivity of the FTO is set to  $142.8 \text{ S m}^{-1}$  (Fig. S2 F).

We note that since the model only scales the conductivity with the z-domain thickness and we do not change the size of the x/y domains, including an anisotropic conductivity for the FTO would be more accurate. Our isotropic simulations therefore result in an over estimation of the potential drop, since current moving in the z-domain will exhibit higher resistances than for the true scale of our FTO substrate. However, for a z-domain size of 0.25 cm and specific conductivity of  $57.12 \text{ S m}^{-1}$ , we calculated that the over-estimation is only limited to less than 3% for a current density of  $3 \text{ mA cm}^{-2}$ . We therefore proceeded with the isotropic scaling of conductivity in our model.

2. A constant current density boundary condition was set at the  $5 \times 10 \text{ cm}$  area at the center of the rectangle and regions between Ni lines (see Fig. S2 B and C) to describe the FTO/BiVO<sub>4</sub> interface. We assumed homogeneous distribution of current at this interface of  $3 \text{ mA cm}^{-2}$ .
3. A constant potential boundary condition was set at the 2 cm region along the outer edge of the rectangle (see Fig. S2 D) to describe the electrical contact. The potential was set to zero at this contact. In the case of Ni-lines modified FTO, the same boundary condition was set at all Ni lines with 1 mm width and 50 mm length (see Fig. S2 E).

Supporting Information

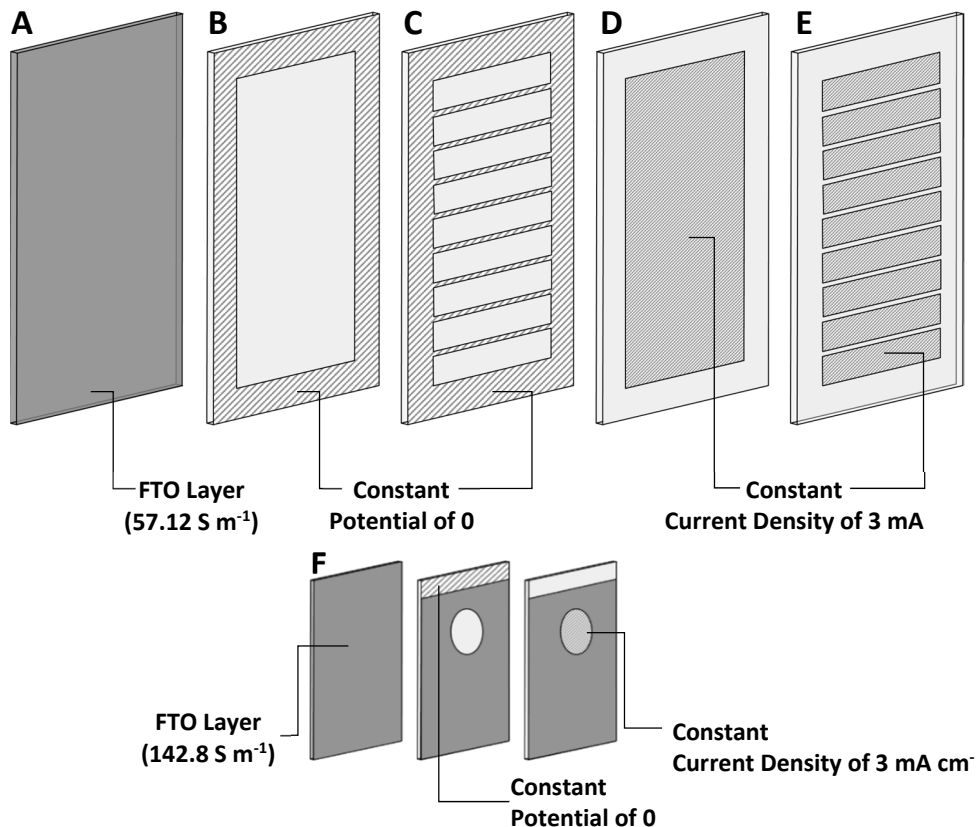


**Figure S2.** Illustration of the 3D model and marked boundary conditions for the simulations of the potential drop across a (A-E) large and (F) small area FTO electrodes.

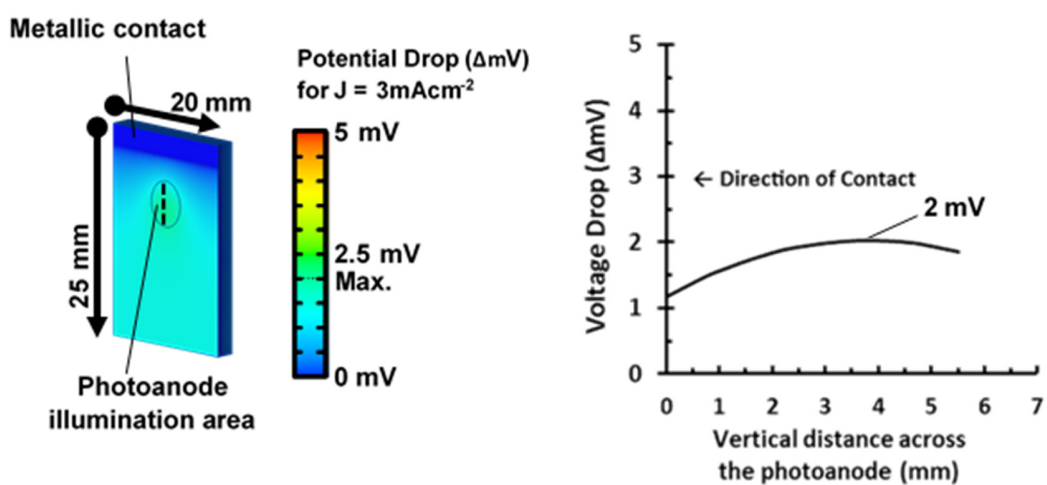


**Figure S3.** Colour gradient plots and graphical plots of the simulated potential distribution across the small area ( $0.24 \text{ cm}^2$ ) photoanode with a current density of  $3 \text{ mA cm}^{-2}$ .

## Supporting Information

### **Supplementary Note S3: Calculation of the potential drop ( $V_{drop}$ ) between the nickel lines**

The maximum potential drop within a large area photoanode modified with nickel lines can be calculated using the simple model shown in Fig. S4, under the following assumptions:

- All nickel lines are at the same potential (no resistive losses within the Ni)
- The photogenerated current density is uniformly distributed over the electrode area
- The current runs perpendicular to the Ni lines and edge effects are ignored

We consider the area in between two adjacent nickel lines; we only need to consider half of the area because of symmetry. The potential exactly halfway in between the two nickel lines is defined to be zero for convenience (i.e.,  $V(y=0) = 0$ ). Since the top and bottom nickel lines each carry half of the photocurrent generated by the area in between, the total current halfway between the lines is zero (i.e.,  $i(y=0)=0$  in Fig. S4).

The absolute photocurrent generated in an area of size  $b \times dy$  (red area in Fig. S4) is given by

$$di = J_{photo} b \, dy \quad (S5)$$

where  $J_{photo}$  is the photocurrent density generated in the material. Integration gives the total photocurrent at position  $y$ :

$$i(y) = \int_0^y J_{photo} b \, dy' = J_{photo} b \, y \quad (S6)$$

The potential drop between the top and the bottom of area  $A$  is given by

$$dV = dR \, i(y) \quad (S7)$$

The resistance  $dR$  between the top and the bottom of the small red-colored element with area  $b \times dy$  in Fig. S4 can be expressed as

$$dR = \frac{R_{sh} dy}{b} \quad (S8)$$

where  $R_{sh}$  is the sheet resistance of the FTO substrate, which is  $7 \Omega/\text{sq}$  in our case. Note: the sheet resistance is defined as the resistance in Ohm between the top and bottom vertices of a square area of a thin film; for a homogeneous film with constant thickness, this value is always the same regardless of the size of the area, as long as it has a square shape.

Combining Eqs. (S6)-(S8) gives:

$$dV = \frac{R_{sh} dy}{b} J_{photo} b \, y = R_{sh} J_{photo} y \, dy \quad (S9)$$

Integration yields the potential at position  $y$ :

$$V(y) = \int_0^y R_{sh} J_{photo} y' \, dy' = \frac{1}{2} R_{sh} J_{photo} y^2 \quad (S10)$$

The maximum potential drop between two nickel lines separated by a distance  $w$  is located at  $y = w/2$ . Its value is thus given by:

$$V_{drop} = V\left(\frac{w}{2}\right) = \frac{1}{8} R_{sh} J_{photo} w^2 \quad (S11)$$

## Supporting Information

The dependence of the voltage drop on the photocurrent density for various nickel line spacings is plotted in Fig. S5. Some values: for a nickel line spacing of 1 cm and a sheet resistance of  $7 \Omega/\text{sq}$ , a photocurrent density  $10 \text{ mA}/\text{cm}^2$  leads to a voltage drop of  $8.75 \text{ mV}$ . Conversely, to limit the voltage drop to  $50 \text{ mV}$  at a photocurrent density of  $3 \text{ mA}/\text{cm}^2$ , the line spacing needs to be less than  $4.4 \text{ cm}$ .

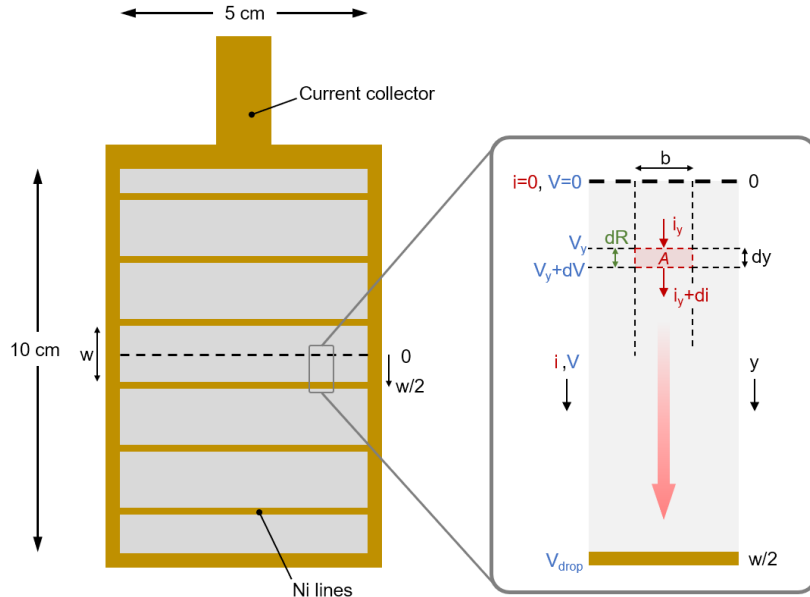


**Figure S4.** Schematic representation of the large-area FTO substrate with conducting Ni lines. The right-hand panel illustrates the calculation of the potential drop in Supplementary Note S3.

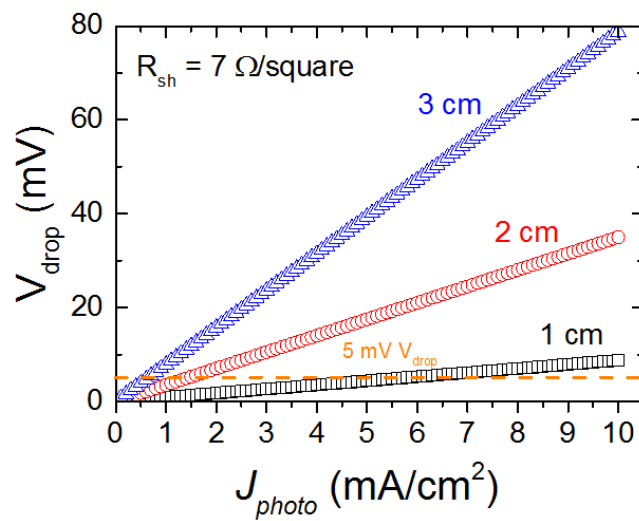


**Figure S5.** Calculated potential drop within a single area in between two adjacent nickel lines (gray areas in left-hand panel of Fig. S4). See Supplementary Note S3 for calculation details.

## Supporting Information

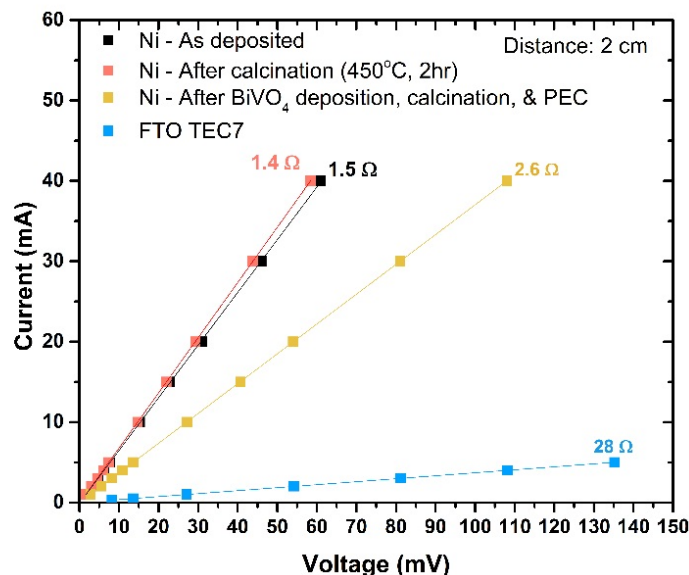


**Figure S6:** Current-voltage measurements for Ni lines deposited on FTO. These measurements were taken using two points, separated by a distance of 2 cm, on a single Ni line. The slope of the curves show the resistances of the Ni lines directly after deposition, after calcination for 2 hours at 450°C in air, and after deposition of SnO<sub>2</sub>/BiVO<sub>4</sub> by spray pyrolysis followed by calcination for 2 hours at 450 °C in air and then PEC measurements in 2 M KP<sub>i</sub>. The increase in resistance for the lines covered by BiVO<sub>4</sub> is most likely due to the acid etching used to remove the SnO<sub>2</sub>/BiVO<sub>4</sub> layer from the contact points. All Ni lines show at least 20 times lower resistance than a corresponding measurement on bare FTO. The measurements were carried out using a Keithley 2401 source meter.

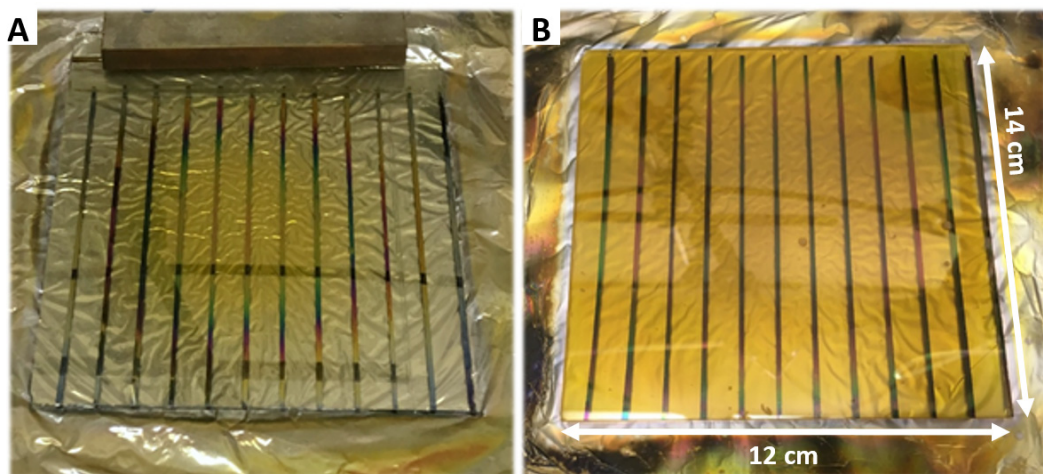


**Figure S7.** Appearance of the large area W:BiVO<sub>4</sub> photo anodes deposited onto TEC 7 FTO substrates with Ni lines from spray pyrolysis, either using **(A)** a spray rate of 1-1.5 mL per cycle (5 s spray) or **(B)** a spray rate of 2-2.5 mL per cycle. The lower spray rate clearly shows smaller deposition coverage.

Supporting Information

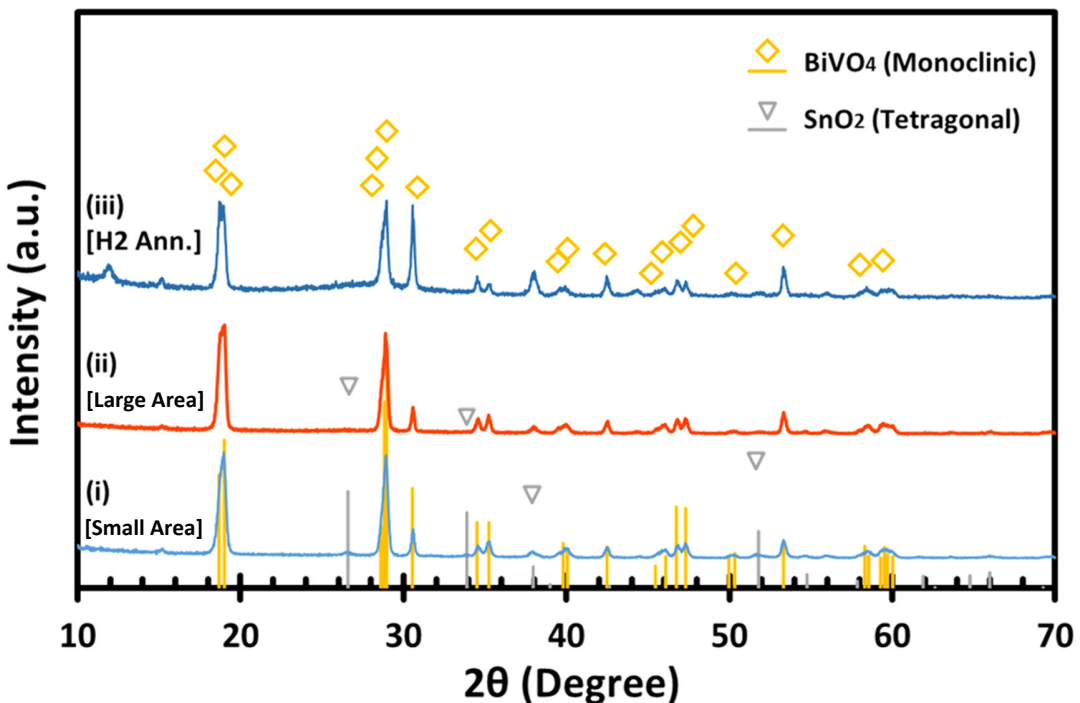


**Figure S8.** Thin film X-ray powder diffraction pattern of the W:BiVO<sub>4</sub> deposited onto SnO<sub>2</sub> coated FTO substrates. Analysis of a section of a sample (i) deposited on a small area ( $2\text{ cm}^2$ ), (ii) deposited on a large area ( $50\text{ cm}^2$ ) and (iii) of a small area sample annealed in 5% H<sub>2</sub> / 95 % Ar for 10 min. at 300 °C. The diffractograms are assigned to the reference peaks for monoclinic BiVO<sub>4</sub> (yellow), PDF #14-0688, and tetragonal SnO<sub>2</sub> (grey), PDF #41-1445.

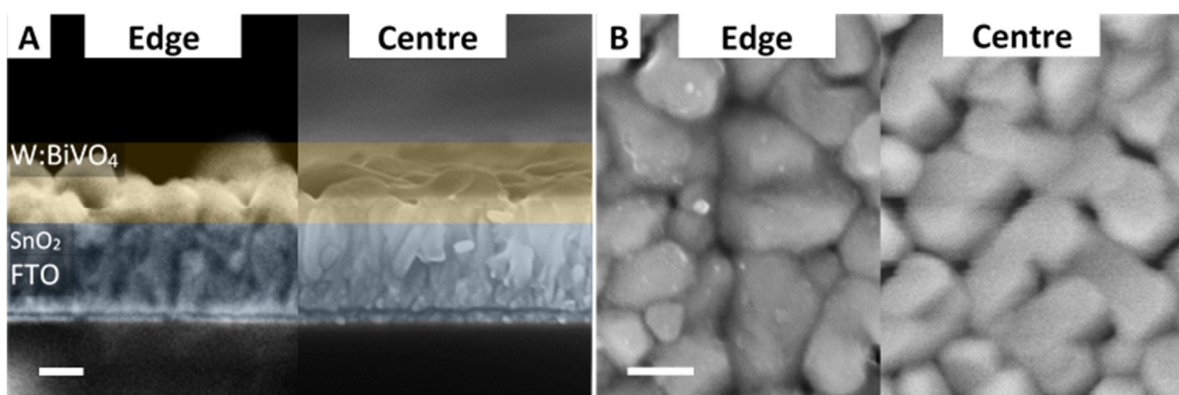


**Figure S9.** (A) Cross section of the centre and edge region and (B) top view of the edge region SEM images of the large area ( $50\text{ cm}^2$ ) W:BiVO<sub>4</sub> deposited onto SnO<sub>2</sub> coated FTO substrates (Scale bar: 200 nm).

Supporting Information

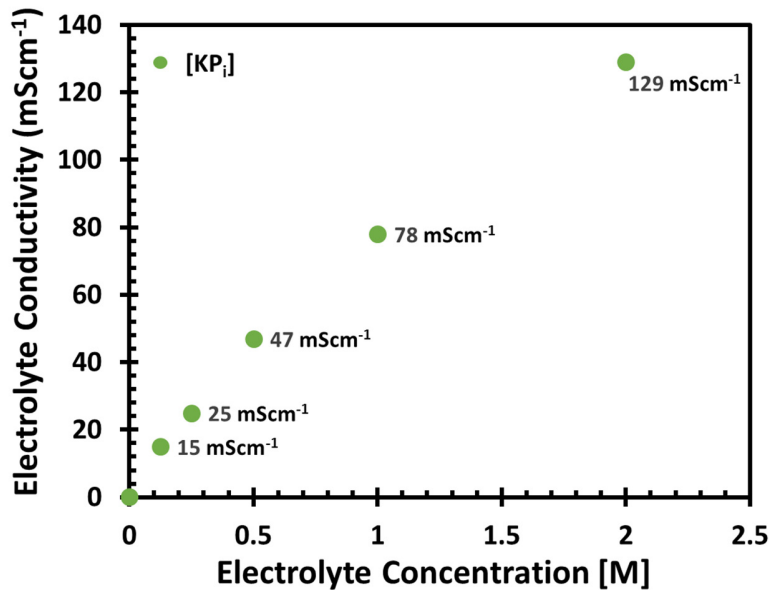


**Figure S10:** Electrolyte conductivity measured as a function of  $KP_i$  concentration at pH ~7.

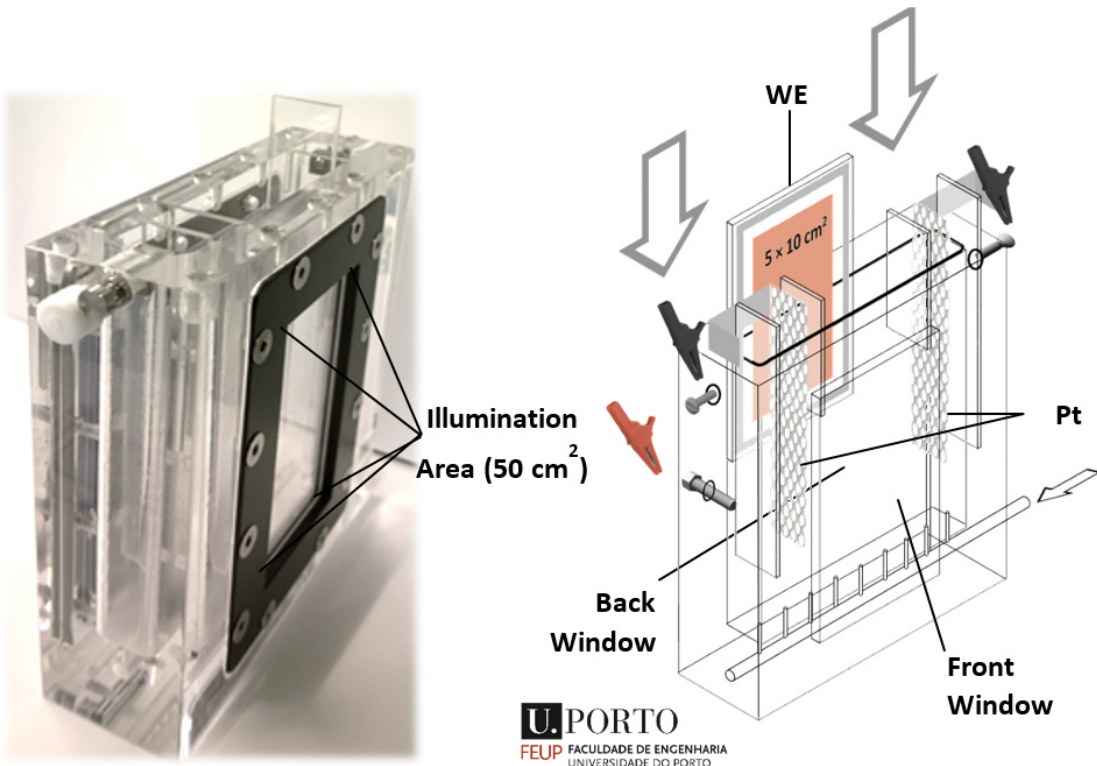


**Figure S11.** Photograph (left) and schematic (right) of the optimized modular cell design which can encase the 2 SHJ PV modules, as well as, the large area ( $50\text{ cm}^2$ ) photo electrodes in either a single or dual photo electrode configuration.

Supporting Information

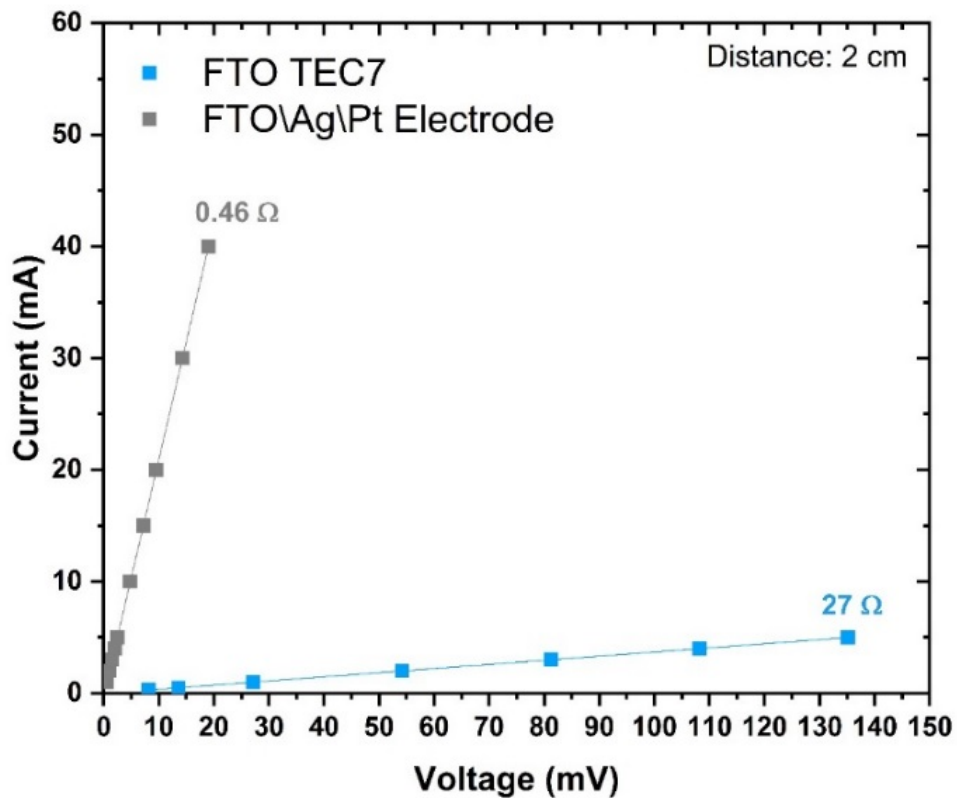


**Figure S12:** Current-voltage measurements of blank FTO (TEC 7) and electrodeposited FTO\Ag\Pt electrodes. The measurements were taken using two points, separated by 2 cm, in the middle of a  $40 \text{ cm}^2$  sample. The measurements were carried out using a Keithley 2401 source meter.

Supporting Information

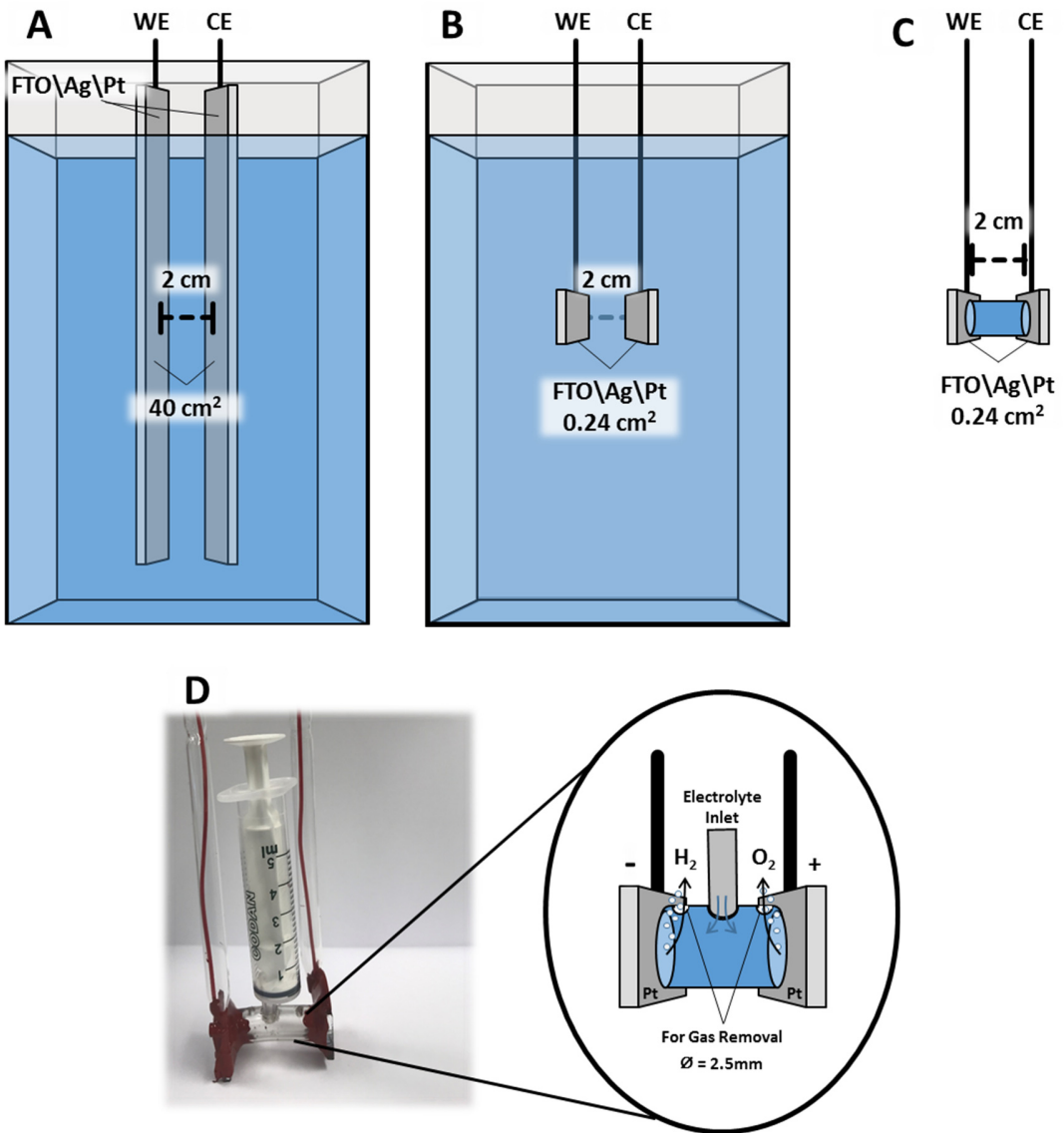


**Figure S13.** Schematics presenting electrodes arrangement used to measure the current-voltage curves for the large ( $40 \text{ cm}^2$ ) and small area ( $0.24 \text{ cm}^2$ ) platinized electrodes. **(A)** Large area Pt electrodes in a large electrolyte volume. **(B)** Small area Pt electrodes in a large electrolyte volume. **(C)** Small area Pt electrodes in a restricted cell volume. **(D)** Photograph and illustration presenting the small area 'restricted' cell design.

Supporting Information

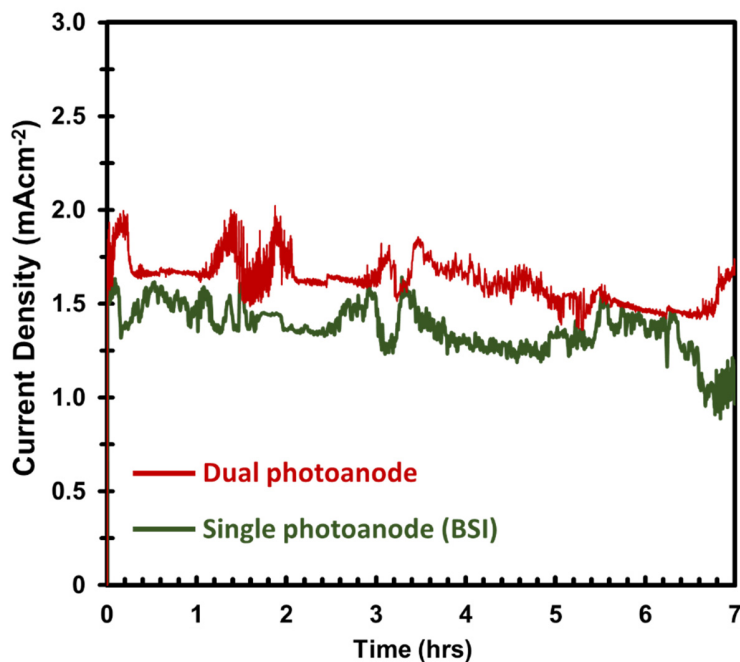


**Figure S14.** Long term stability tests for the stand-alone tandem PV-PEC device in either the single (green) or dual (red) photoanode configuration, under AM 1.5 illumination. The device structure consists of W:BiVO<sub>4</sub>(BSI)/Electrolyte(pH:7, 2.0 M KPi)/W:BiVO<sub>4</sub>(FSI)/2 SHJ-PV/2Pt. Throughout each test the electrolyte was purged with N<sub>2</sub> gas.

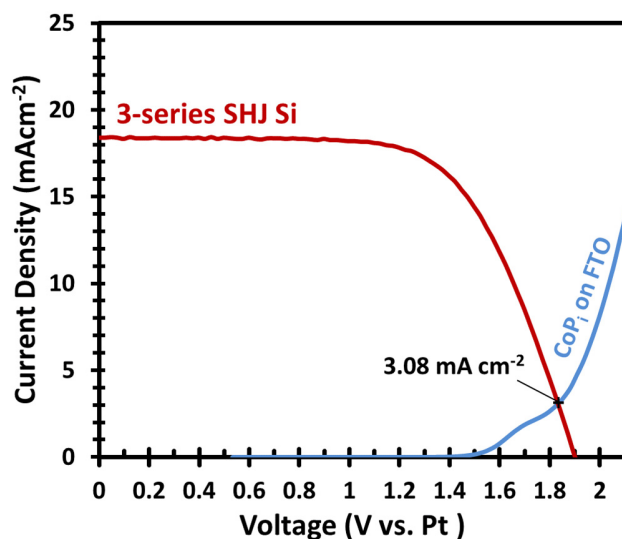


**Figure S15:** J-V curves and working point for the 3xSHJ-Si PVs and a  $0.24 \text{ cm}^2$  sample of CoPi electro-deposited onto FTO. Water splitting is possible by placing three SHJ-Si cells in series, but the current is significantly lower than the  $5.12 \text{ mA cm}^{-2}$  that is obtained in combination with a dual BiVO<sub>4</sub> photoanode.

Supporting Information

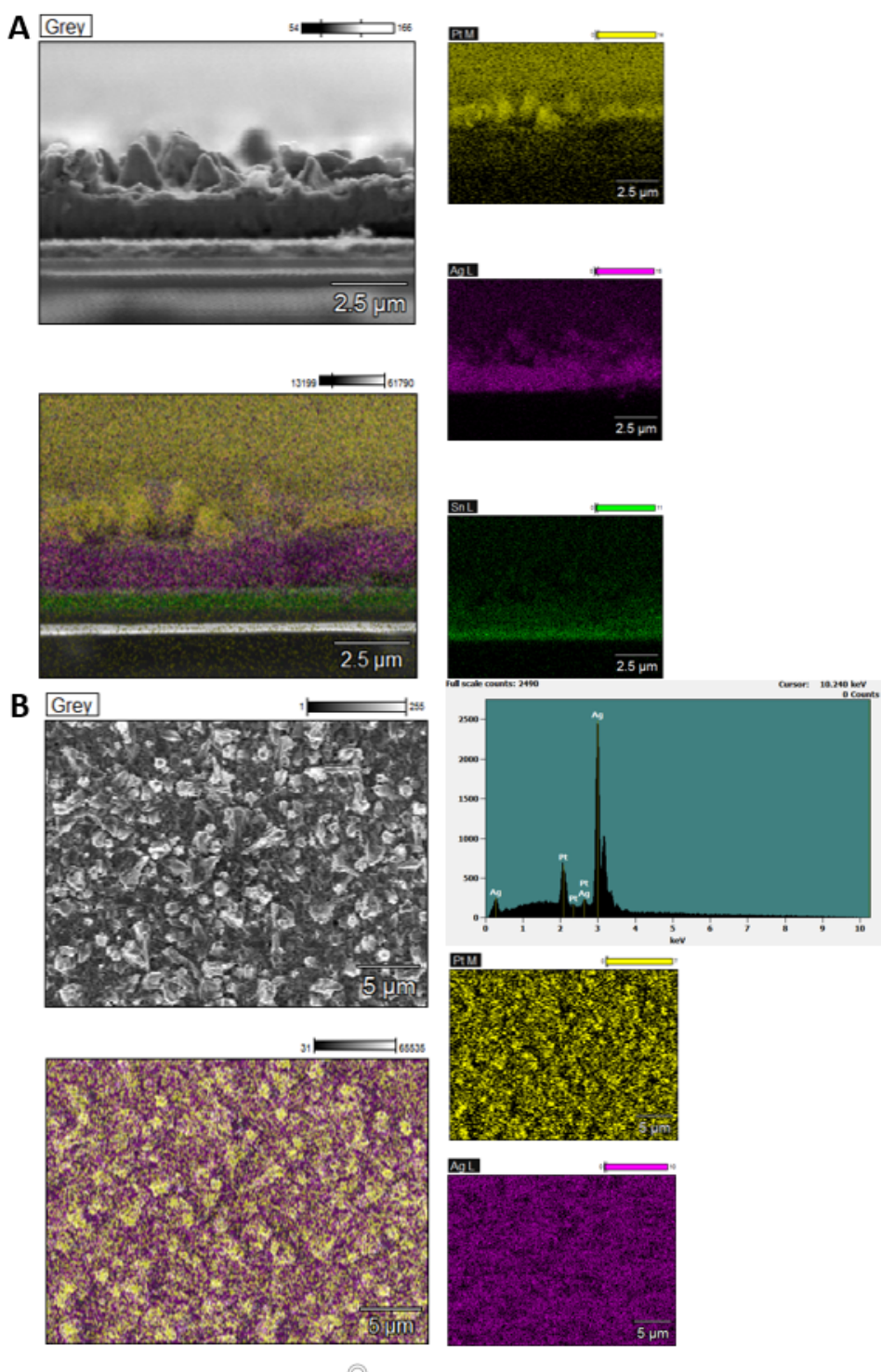


**Figure S16.** **(A)** Cross section and **(B)** top-down SEM images and EDAX spectral images of the glass/FTO/Ag/Pt electrodes, prepared using a chemical treatment method and subsequent electrodeposition of Ag and Pt. SEM micrographs and EDAX spectra were collected using a 10 keV acceleration voltage.

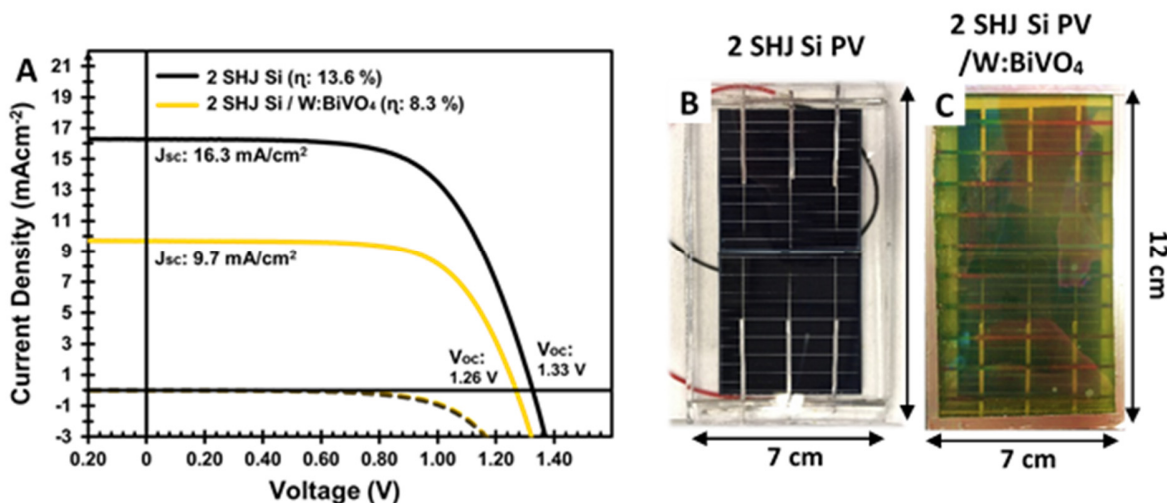


**Figure S17.** **(A)** J-V characteristics under dark (dashed line) and AM 1.5G, 100 mW cm<sup>-2</sup> illumination (solid line) for the 50 cm<sup>2</sup> devices comprising of either **(B)** 2 x SHJ modules (black) or **(C)** the integrated 2 x SHJ modules with a single W:BiVO<sub>4</sub>/SnO<sub>2</sub>/FTO sample, with Ni gridlines, placed on top (yellow).

**Table S1.** Device performance characteristics of the integrated 2 x SHJ module with and without BiVO<sub>4</sub>.

PV/Photoanode Device:	2 SHJ PV	2 SHJ PV/W:BiVO <sub>4</sub>
$J_{sc}$ [mAcm <sup>-2</sup> ]	16.28	9.69
$V_{oc}$ [V]	1.33	1.26
FF [%]	63.0	67.1
Eff. [%]	<b>13.61</b>	<b>8.26</b>
$V_{mp}$ MPP [V]	0.97	0.96
$J_{mp}$ MPP [mAcm <sup>-2</sup> ]	14.0	8.6
MPP [mWcm <sup>-2</sup> ]	13.6	8.3
Series Resistance [ $\Omega\text{cm}^2$ ]	15.4	18.8
Shunt Resistance [ $\text{k}\Omega\text{cm}^2$ ]	22.0	12.1

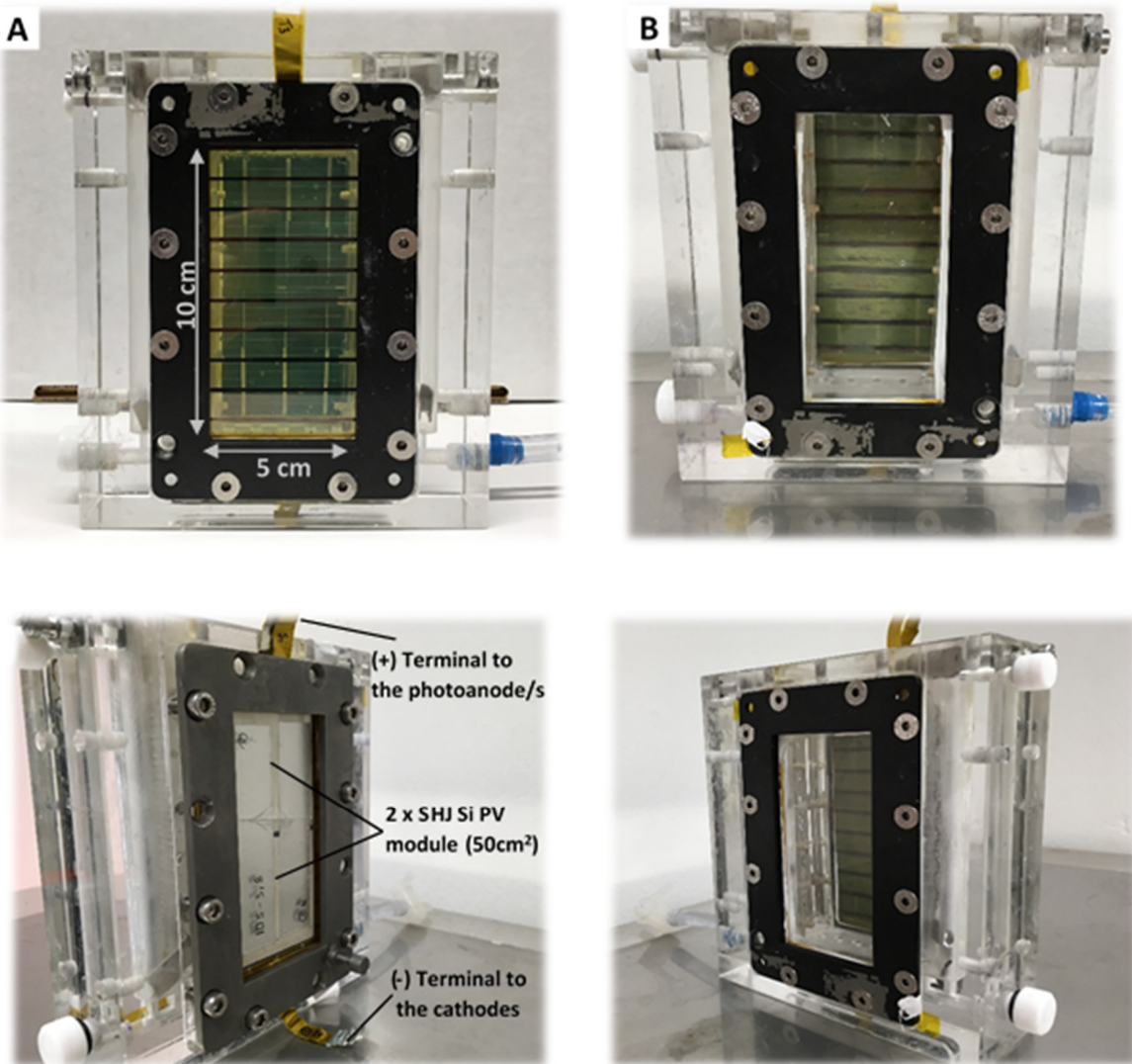


**Figure S18.** Photograph of the large area integrated PV-PEC device consisting of a  $50\text{ cm}^2$  2 x SHJ PV module, with the optimized  $50\text{ cm}^2$  W:BiVO<sub>4</sub> photoanodes, and Pt coated counter electrodes. Photo anodes can be switched between either the front **(A)**, or back **(B)** window of the cell to test for different device configurations. **(C)** Back view PV-PEC device with the view of the 2 x SHJ PV module interconnections. **(D)** Side view of the PV-PEC device.

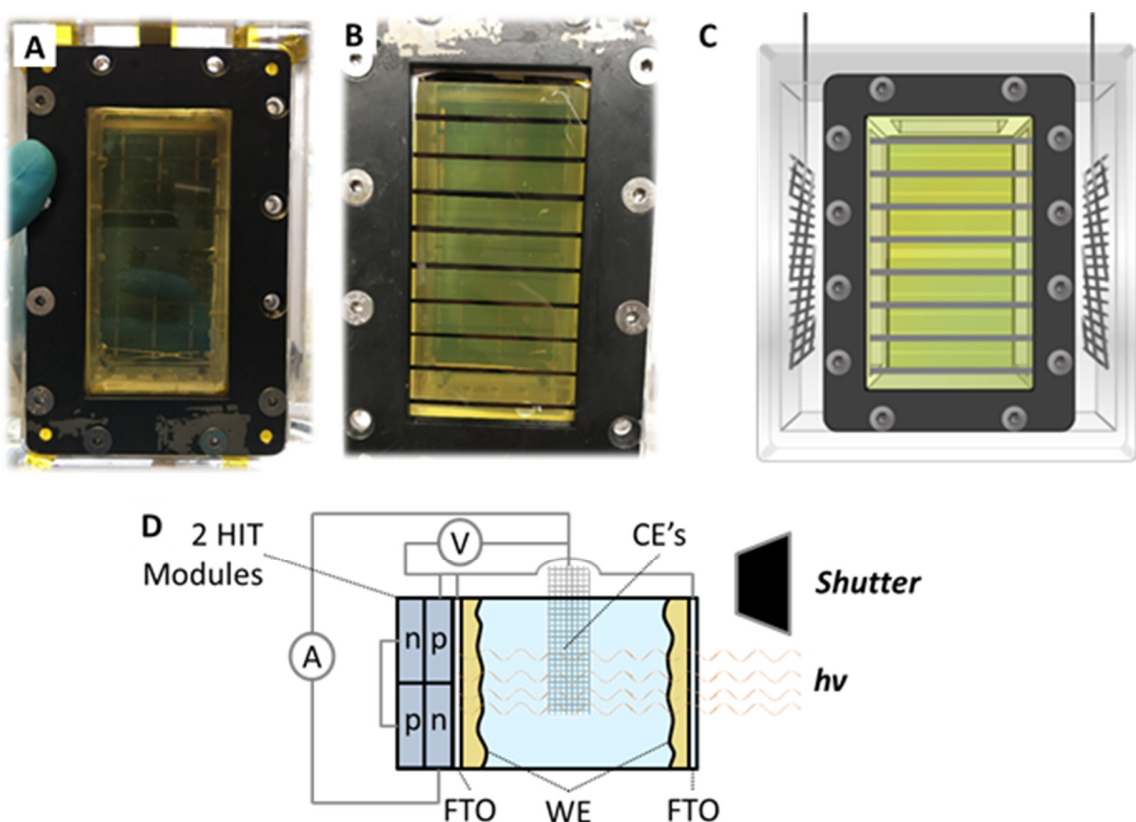


**Figure S19.** Photograph of the large area ( $50 \text{ cm}^2$ ) integrated PV-PEC device in the dual photo anode configuration with a device structure of W:BiVO<sub>4</sub>(BSI)/Electrolyte/W:BiVO<sub>4</sub>(FSI)/2 SHJ-PV/Pt, **(A)** without and **(B)** with Ni gridlines. **(C)** Schematic of the  $50 \text{ cm}^2$  cell from a front view of the device. **(D)** A simplified scheme of the measurement setup for the stand-alone water splitting device.

Supporting Information

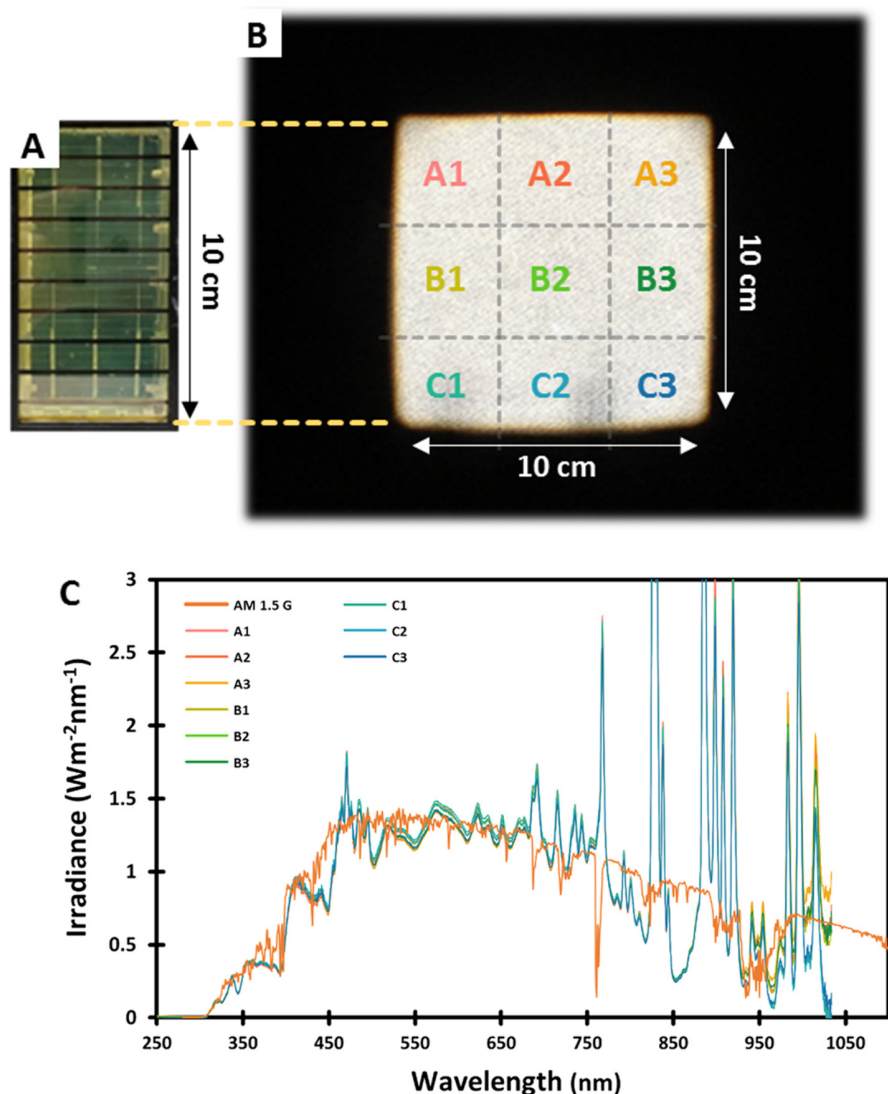


**Figure S20.** Measured spatial distribution of the irradiance generated by the Wacom super solar simulator WXS-50S-5H, AM 1.5G. **(A–B)** A photograph of the large area  $\text{BiVO}_4$  PV-PEC device, the illumination area and the 9 regions measured. **(C)** Irradiance spectra of the 9 regions measured using a Calibrated Ocean Optics USB2000+RAD spectrometer, compared with the standard AM 1.5 G solar irradiance spectrum.<sup>1</sup>

## Supporting Information

**Table S2.** Integrated irradiance (between 400 and 900 nm) taken from the different spectra measured as shown in Figure S20.

Position	Integrated Irradiance (W/m <sup>2</sup> ) 400 to 900 nm
A1	633.5
A2	634.3
A3	639.0
B1	635.2
B2	635.5
B3	635.9
C1	638.1
C2	636.0
C3	635.1
AM 1.5 G	635.7
Range: ± 1 %, Mean: 635.8	

## References:

1. ASTM G173-03(2012), Standard Tables for Reference Solar Spectral Irradiances: Direct Normal and Hemispherical on 37° Tilted Surface, ASTM International, West Conshohocken, PA, 2012, [www.astm.org](http://www.astm.org). DOI: 10.1520/G0173-03R12